

Nanoscale

Accepted Manuscript



This is an *Accepted Manuscript*, which has been through the Royal Society of Chemistry peer review process and has been accepted for publication.

Accepted Manuscripts are published online shortly after acceptance, before technical editing, formatting and proof reading. Using this free service, authors can make their results available to the community, in citable form, before we publish the edited article. We will replace this *Accepted Manuscript* with the edited and formatted *Advance Article* as soon as it is available.

You can find more information about *Accepted Manuscripts* in the [Information for Authors](#).

Please note that technical editing may introduce minor changes to the text and/or graphics, which may alter content. The journal's standard [Terms & Conditions](#) and the [Ethical guidelines](#) still apply. In no event shall the Royal Society of Chemistry be held responsible for any errors or omissions in this *Accepted Manuscript* or any consequences arising from the use of any information it contains.

Engineering Excitonic Dynamics and Environmental Stability of Post-Transition Metal Chalcogenides by Pyridine Functionalization Technique

Xiuqing Meng^{1,2}, Anupum Pant¹, Hui Cai¹, Jun Kang³, Hasan Sahin², Bin Chen¹, Kedi Wu¹, Sijie Yang¹, Aslihan Suslu¹, F. M. Peeters³, and Sefaattin Tongay¹

¹ School for Engineering of Matter, Transport and Energy, Arizona State University, Tempe, AZ 85287, United States

² Research Center for Light Emitting Diodes (LED), Zhejiang Normal University, Jinhua 321004, P. R. China

³ Department of Physics, University of Antwerp, Groenenborgerlaan 171, Antwerpen B-2020, Belgium

⁺To whom correspondence should be addressed: E-mail: Sefaattin.Tongay@asu.edu

Abstract

Owing to their strong photon emission, low excitonic binding energies, and nearly-ideal band offset values for water splitting reactions, direct gap quasi-2D gallium chalcogenides are potential candidates for applications in energy harvesting, optoelectronics, and photonics. Unlike other 2D materials systems, chemical functionalization of gallium chalcogenides is still at its seminal stages. Here, we propose vapor phase pyridine intercalation technique to manipulate optical properties of gallium chalcogenides. After functionalization, the excitonic dynamics of quasi-2D GaSe change significantly as evidenced by an increase in integrated PL intensity and emergence of a new emission feature that is below the band edge. Based on our DFT calculations, we attribute these to formation of bound exciton complexes at the trap sites introduced by chemical reaction between pyridine and GaSe. On the contrary, pyridine functionalization does not impact the optical properties of GaTe, instead treats GaTe surface to prevent oxidization of tellurium atoms. Overall, results suggest novel ways to control properties of gallium chalcogenides on demand and unleash their full potential for a range of applications in photonics and optoelectronics.

Keywords:

Two dimensional materials, surface functionalization, optical spectroscopy, post-transition metal chalcogenides

Recently, post-transition metal chalcogenides (PTMCs) have emerged as alternative 2D semiconducting materials owing to their strong second harmonic generation¹⁻³, unusual band renormalization effects⁴⁻⁷, low excitonic binding energies⁴⁻⁶, and direct gap nature in the few-layer form⁵. PTMCs have the chemical formula of MX where M post-transition metals (e.g. Ga, In, Tl) are covalently bonded to chalcogen atoms (e.g. S, Se, and Te) and each layer has X-M-M-X atomic arrangement as shown in Figure 1a. Similar to other layered materials, they can be isolated to mono- and few-layers using standard mechanical exfoliation technique, or alternatively can be grown in 2D and quasi-2D form using variety of vapor transport techniques^{4, 8-11}. More recently, these materials have attracted much interest and 2nd harmonic generation effects^{2, 3}, photodetectors^{8, 10, 12}, and FETs^{8, 9, 13} applications have been experimentally demonstrated using gallium chalcogenides (M=Ga) as active materials.

In the bulk form, direct gap GaSe and GaTe display rather strong photoluminescence (PL) peak appearing at 2.0 eV and 1.65 eV, respectively, but goes from direct to indirect transition as they are isolated to monolayers^{8, 10, 13, 14}. In this regard, light emission from 2D-PTMCs requires phonon participation in the exciton recombination process which is rather inefficient for any realistic device applications relying on strong absorption or emission of photons. However, few-layered (quasi-2D) GaX (X=Se and Te) sheets are potential candidates for optoelectronics applications for the following reasons: 1. They are direct gap semiconductors, emitting and absorbing photons rather efficiently, 2. They are mechanically flexible similar to TMDCs and graphene, 3. they offer advantages over group-VI TMDCs as they possess low exciton binding energies, and 4. Possess nearly ideal band offsets for water-splitting reactions¹⁵. Since quasi-2D direct gap GaX semiconductors are not strictly in 2D, their exciton binding energies are significantly smaller (~50 meV) than that of TMDCs (~400-700 meV) due to reduced quantum confinement effects¹⁶⁻²¹. This implies that energy harvesting devices concepts (photovoltaics) can be easily applied to GaX without any need for large energy for separating e-h pairs. However, for realistic device applications, it is required to develop novel routes to manipulate their properties at will.

Previously, intercalation technique has been applied to different kinds of layered material systems such as graphite / graphene²²⁻²⁷, MoS₂²⁶, and WSe₂²⁸, where group IA (Li and K) and group VIIA (Br₂ and I₂) atoms/molecules were intercalated across the layers to achieve 2H- to T-phase semiconducting to metallic transition as well as to charge the host material either *n*- or *p*-type depending on the intercalating species²⁹. But these intercalant atoms and molecules are only applicable to graphitic and TMDCs, and rather ineffective for PTMCs as a result of stronger interlayer coupling preventing these atoms to diffuse between layers^{29, 30} and Na intercalation process was shown to have rather minimal effect or completely deteriorate material itself³¹.

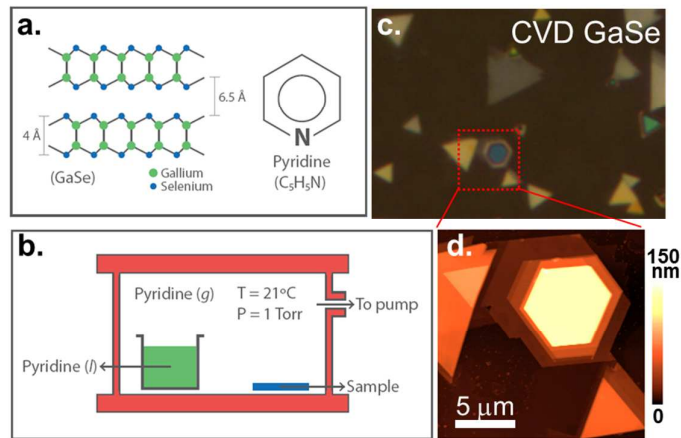


Figure 1 Schematic of intercalation process **a.** Chemical structure of gallium chalcogenides and pyridine molecules **b.** Schematics of the pyridine intercalation setup. **c.** Optical and **d.** AFM image taken from CVD GaSe sheets.

Here, we report on controlling optical and excitonic properties of GaSe and GaTe by organo-intercalation technique using pyridine organic molecules (C_5H_5N). Results show that pyridine molecules intercalate between GaSe layers as evidenced by increased interlayer spacing (**Figure 2a-d**) measured by atomic force microscopy (AFM) and enhanced interlayer coupling strength from Raman spectroscopy measurements. Optical spectroscopy measurements show that excitonic dynamics and PL of GaSe largely change after intercalation process. In contrast to GaSe with relatively weaker interlayer interaction, pyridine molecules do not diffuse across GaTe layers, but instead functionalize GaTe surface which results in much improved environmental stability and Raman spectrum. Overall findings herald new venues to control material properties of quasi-2D PTMCs which are potential candidates in optoelectronics, particularly energy harvesting devices, owing to their smaller exciton binding energies and nearly ideal band alignment for photo-electrochemical cell (PECs) applications¹⁵.

Sample preparation and pyridine treatment Bulk PTMCs crystals were grown using conventional Bridgman-Stockbarger method⁴, and few-layer GaSe and GaTe sheets were isolated from their bulk counterparts using mechanical exfoliation onto 295 nm thick thermal SiO_2 on Si (SiO_2/Si) substrates. Chemical vapor deposited (CVD) GaSe sheets were synthesized (**Figure 1c-d**) by transporting bi-products from a mixture of Ga_2Se_3 and GaSe powders (molar ratio 1:50) placed in the middle of the furnace at $750^\circ C$, onto sapphire (c-cut) substrates placed downstream in a relatively cooler zone, at least $\sim 10-30^\circ C$ below $750^\circ C$. Argon was chosen as the carrier gas (10scm) due to its chemical inertness, and the total growth time was 10 minutes. During the synthesis, chamber pressure was maintained at 10 Torr. Pyridine intercalation was performed at $21^\circ C$ in a vacuum chamber containing pyridine liquid solution (volume ~ 0.5 mL) and exfoliated GaX (*e.g.* GaSe and GaTe) flakes on SiO_2/Si .

The vacuum chamber was pumped down to low pressures to facilitate vaporization and a pressure of 1 Torr was maintained during the intercalation process (**Figure 1b**). As a notation, we will refer to pyridine treated GaSe and GaTe 2D sheets as P-GaSe and P-GaTe, respectively for convenience.

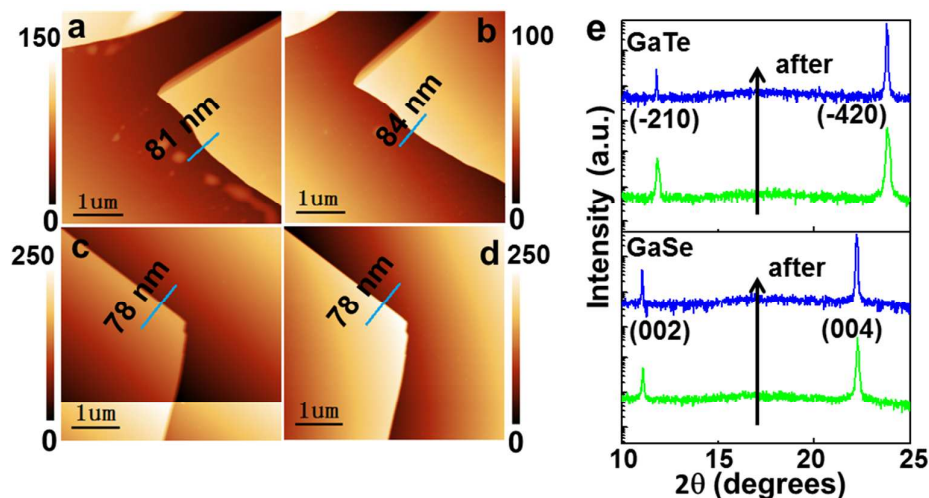


Figure 2 Structural changes after pyridine treatment. AFM images of exfoliated a-b. GaSe and c-d. GaTe before and after pyridine intercalation, respectively e. XRD patterns of the gallium chalcogenides before and after the pyridine treatment.

To understand the changes in the surface morphology and the thickness of the 2D sheets, atomic force microscopy (AFM) measurements were performed before and after the pyridine treatment. Pristine GaSe exhibits rather smooth surface which measures 81 nm in thickness (**Figure 2a**). After intercalation, however, its thickness increases nearly by 4% up to 84 nm, which corresponds to ~4% lattice expansion. Here, we note that this change has been confirmed on a large number of GaSe sheets, and in each measurement, the AFM tip was calibrated for highest accuracy. Typically, when guest species (e.g. Li or K) intercalate between the layers of hosting lamellar material system, such as graphitic materials, they form periodic sequences / arrangements of native and guest layers, forming staged structures which can be identified by the emergence of new x-ray reflection peaks in the x-ray diffraction (XRD) pattern^{27, 29, 30}. However, considering relatively small changes in the c-axis and unchanged x-ray diffraction pattern (XRD) (Figure 2e bottom a=b=0.3767 nm, c=1.5957 nm of GaSe [JCPDS 37-931]), we conclude that P-GaSe is not staged, but instead pyridine molecules are randomly distributed across the layers. This is rather similar to bromine, iodine, or other organic intercalation compounds for different lamellar material systems where staging is energetically not favorable^{22, 27, 32}.

In addition to AFM measurements, the presence of guest pyridine molecules can also be detected by micro-Raman measurements, which provides invaluable information regarding to interlayer coupling from the changes in the vibrational properties of the

material itself. In Figure 3a-b, Raman spectra taken from exfoliated and CVD grown GaSe sheets are depicted before and after intercalation. Overall spectra display four most prominent first order Raman peaks located at 138, 217, 254, and 312 cm^{-1} , respectively, which correspond to A''_1 , E'' , $E'_{(\text{LO})}$, and A'_1 vibrational modes, consistent with the reported values^{4, 8, 13}. Out of these four peaks, A''_1 mode is most sensitive to the restoring forces (interlayer coupling) acting on the adjacent layers. In fact, out-of-plane A''_1 peak position has been identified as a reliable parameter to measure the thickness of the 2D sheets, mainly because the interlayer coupling shows considerable changes going from bulk to monolayers and the A''_1 peak position follows a trend with the material thickness^{33, 34}. After pyridine molecules are intercalated between the layers, the restoring forces acting on individual GaSe layers (by inserted pyridine molecules) increases, thereby stiffening the A''_1 mode from 138.8 to 139.4 cm^{-1} as confirmed by our Raman measurements (Fig. 3a-b). Here, it is worthwhile to mention that if the layer – layer distance were to increase without any foreign species intercalated between the layers, one would expect to observe softening in the Raman mode frequencies due to reduced interlayer interaction and restoring forces. When intercalants are present between layers, two opposing effects occur simultaneously: Intercalants increase the interlayer spacing (reducing the restoring force) and tightly interact with the hosting matrix increasing the restoring force. Observed results imply that the latter effect (interaction between layers and foreign molecules) dominate over slight increase in lattice spacing, thereby stiffening the out-of-plane Raman mode. Indeed, similar results have been observed in other intercalation compounds and such changes have been attributed to magnitude of the interplay between intercalant – host matrix interactions^{35, 36}.

After discussing changes in GaSe, next we discuss our results for P-GaTe. In contrast to our findings for GaSe, total thickness, XRD ($a = 1.745$ nm, $b = 1.047$ nm, $c = 0.409$ nm and $\gamma = 104.5^\circ$ of GaTe [JCPDS No. 33-571]), and the Raman spectrum display no change after pyridine treatment, implying that the intercalation technique is not effective for tuning the properties of GaTe (Figure 2e). It is anticipated that the interlayer coupling strength of GaTe is much greater than that of GaSe, owing to larger Bohr radius of Te atoms, and thus pyridine diffusion process is less likely to happen in GaTe compared to GaSe. To test this, we have performed DFT calculations to determine the interlayer binding energy, which is defined as the energy difference between bulk material and isolated monolayers, for GaSe and GaTe. In agreement with above discussions, interlayer coupling energy of GaTe (-1.936 eV/nm²) is much stronger than that of GaSe (-1.576 eV/nm²), and thus, GaTe sheets are prone to pyridine intercalation process. Even though pyridine molecules do not participate in the intercalation process, they interact with the highly oxidizing GaTe surface (**Figure S1**) to increase the material's environmental stability. These findings will be discussed later in the article.

Changes in optical properties of PTMCs after pyridine treatment Next, we focus on the effects of pyridine treatment on the optical properties of gallium chalcogenides. **Figure 3c-d** shows the PL spectrum taken on exfoliated and CVD GaSe sheets before and after the intercalation process: It can be seen that the overall PL peak increases in intensity and peak shape changes in a way that a new emission line appears at 1.969 eV which is ~ 25 meV below the band edge at 1.997 eV. This implies that pyridine molecules largely modulate the excitonic dynamics (lifetimes) as well as exciton complexes (e.g. free vs bound excitons). Earlier results on TMDCs (MoS₂, MoSe₂, MoTe₂, and WSe₂) have shown that the interaction between 2D materials and such highly polar molecules as O₂, H₂O, and Li effectively changes the surface carrier concentration, which in return manifested itself as neutral (X^0 : eh) to charged ($X^{+/-}$: eeh or ehh) transition^{37, 38}. For 2D TMDCs, the energy splitting between X^0 and $X^{+/-}$ is in the order of 20-40 meV³⁹, but this is largely unknown for 2D and quasi-2D PTMCs⁴⁰. One possible explanation is that the peak splitting in Figure 3c is associated with $X^0 \rightarrow X^{+/-}$ crossover mediated by pyridine-GaSe charge transfer. In this case, the low energy peak (labeled as A) would be attributed to the charged exciton complexes, whereas the high energy peak (B) is from neutral excitons. However, we note that **this is rather unlikely picture** as the trion binding energy is expected to be large (~ 30 meV) only when the system is truly 2D in nature, e.g. when the electron wavefunction is tightly localized and quasi-particle interactions are much enhanced, as previously observed in 2D MoS₂ and MoSe₂³⁹. On the contrary, GaSe sheets in this work are few-layers to 100 nm in thickness, and the binding energy of trions is anticipated to be close to an order of magnitude smaller ($E_{\text{binding}} < 5$ meV) than observed peak splitting (~ 25 meV)⁴⁰.

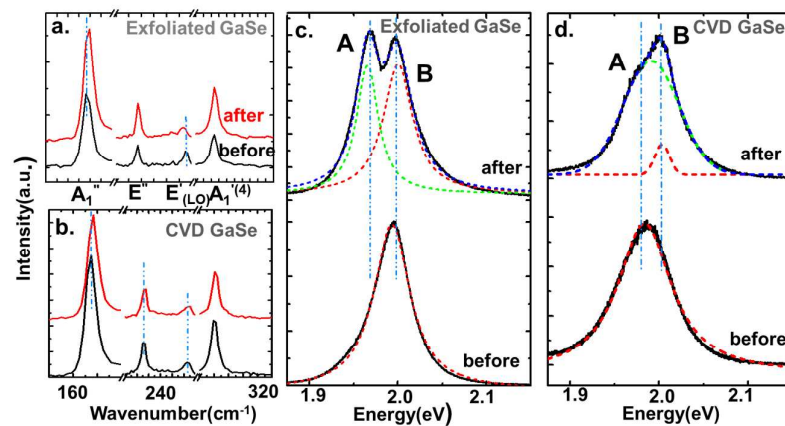


Figure 3 Optical properties of GaSe before and after intercalation Raman spectra of a. exfoliated and b. CVD grown quasi-2D GaSe sheets before and after pyridine intercalation. PL spectra and fitted lines of c. exfoliated and d. CVD grown GaSe before and after intercalation. Peak A and B corresponds to low energy and high energy peaks which are separated by 25 meV.

Another possibility involves mechanical strain induced by guest pyridine molecules and this effect will also be discussed in parallel with other mentioned possible mechanisms to explain the overall PL spectrum. To assess mechanical strain model, we have performed DFT calculations on pristine and P-GaSe sheets (**Figure 4a**). Since pyridine molecules break the periodic unit cell approximation, we have compared the density of states (DOS) of GaSe after pyridine intercalation (**Figure 4a**) to estimate band gap changes. DFT calculations show that the optical band gap increases by 330 meV due to quasi-2D to 2D crossover and band renormalization mediated by the increase in the interlayer spacing, which is more than a decade larger than observed peak splitting (~ 25 meV), and thus mechanical strain itself cannot account for the observed changes in the PL spectrum.

Last possibility is related to presence of bound excitons (X^B): Intercalation process is notoriously known to introduce some degree of the imperfections into the lattice forming donors or acceptors^{27,29}. In the presence of these defect sites, free excitons are efficiently trapped in reduced dimensions (2D), when the electron wavefunction is tightly localized, at the defect / impurity sites. Since two PL peaks are separated by ~ 25 meV, these localized traps are likely to be shallow impurities just below or above the conduction band minimum (CBM) or valence band maximum (VBM), respectively. To confirm our results, we have performed similar measurements on large area 2D-GaSe sheets synthesized by chemical vapor deposition technique (CVD) at 750 °C. **Figure 3d** shows that PL of CVD GaSe sheets already display dominant 'A' peak which are associated with chalcogen (Se) vacancies which are common among CVD grown 2D chalcogenide materials. In this case, pyridine molecules are anticipated passivate vacancy sites after binding at these imperfections to reduce the emission (radiative recombination) of peak A. Indeed, recent report on GaSe has pointed out that bound excitonic features appear at energies red shifted by ~ 40 meV⁷. This agrees well with our observation where the new PL feature also appears $\sim 30-40$ meV below the main emission line. However, future studies on time-resolved photoluminescence measurements from micron-size probing areas might clarify the underlying mechanisms and excitonic dynamics.

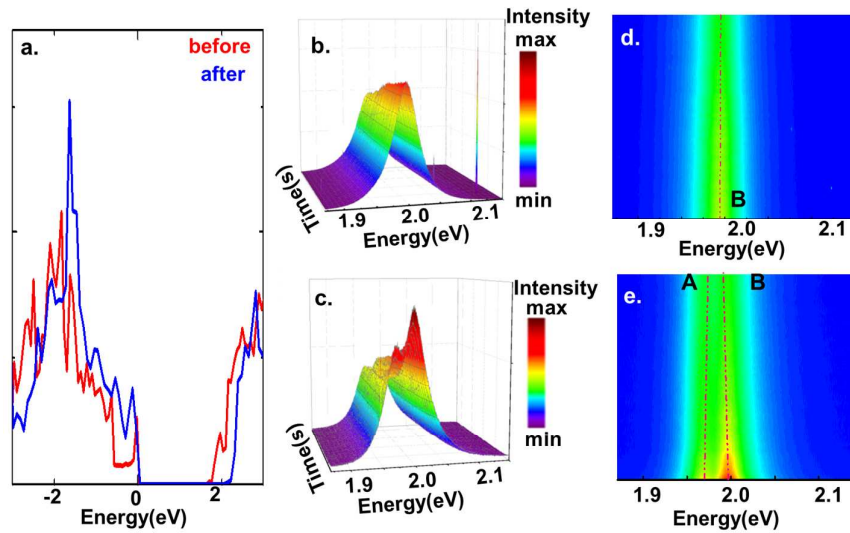


Figure 4 Environmental studies on pyridine treated GaSe sheets a. Density of states (DOS) of pristine and intercalated GaSe sheets. Three dimensional plots of PL spectrum from b. pristine and c. intercalated GaSe and corresponding two dimensional time dependent PL spectra for d. pristine and e. intercalated GaSe sheets. Each PL spectrum data was collected every 5 seconds repeatedly for 15 minutes and plotted in 3D form. Full timescale is 15 minutes in total.

To gain further insight into the neutral exciton – bound exciton complexes, we have performed detailed environmental studies to observe how pyridine intercalation related changes in the material properties evolve over time (Figure 4b-e) that are similar to studies in other 2D material systems⁴¹⁻⁴⁵. More specifically, if the lower energy peak (A) is associated with the bound excitons that are caused by permanent structural imperfections introduced by pyridine, it is anticipated that this new peak will display either negligible time dependence and will still be distinguishable after prolong amount of time. Time dependent PL spectra were collected from pristine and P-GaSe every 5 seconds up to 15 minutes under 488 nm excitation laser and results are shown in Figure 4b, d (pristine) and 4c, e (intercalated). Before discussing our on results on P-GaSe, we point out that the PL spectrum of pristine GaSe is largely unchanged mainly because the GaSe crystal is environmentally stable and its surface does not deteriorate (Figure 4b and d), whereas P-GaSe undergoes significant changes over time (Figure 4c and e). Figure 4e shows a color map of the PL spectrum of P-GaSe as a function of time in which we clearly observe two spectral features whose intensities strongly depend on time. The two peak feature rapidly decays in intensity but the overall integrated PL remains much higher than the pristine GaSe even after couple weeks. More importantly, the low energy feature is still distinguishable after 15 minutes timescale (Figure 4e) or even after three weeks. This implies that the peak A likely to be associated with permanent changes in GaSe, in support of the neutral exciton and bound exciton complexes. Despite our PL 3D-contour plot duration time was limited to 15 minutes to avoid local overheating effects, adversely affecting structure of materials, and power source fluctuations in extended periods of time, detailed environmental

studies were performed within 2 weeks timeframe. Our results point out that GaSe layers remain intact and optical performance remain unchanged after first 10 minutes.

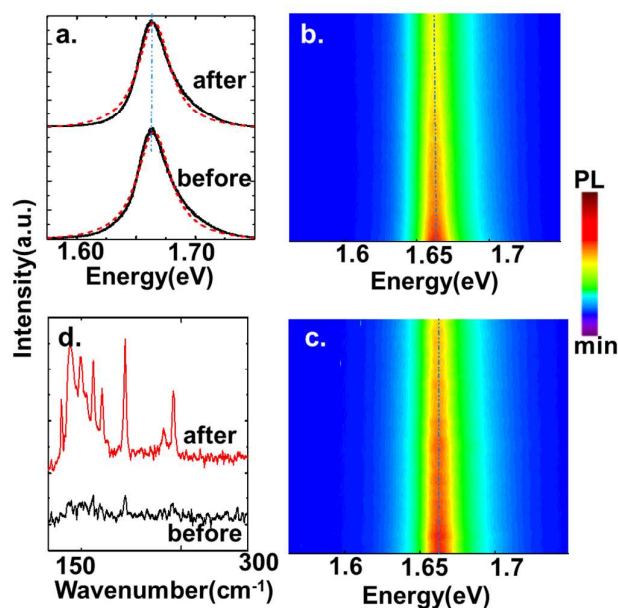


Figure 5 Optical properties of GaTe before and after intercalation. a. PL spectrum of exfoliated GaTe before and after intercalation, b. color map of pristine GaTe PL as a function of time (y axis up to 15 minutes) and c. color map of intercalated GaTe d. Raman spectra of exfoliated GaTe before (black) and after (red) pyridine intercalation, respectively.

After presenting results on GaSe, we discuss the effects of pyridine intercalation on the optical properties of GaTe sheets. From Figure 5a, we observe an emission peak at 1.66eV, which can be attributed to the direct band gap emission (neutral excitons), and this peak remains largely unchanged both in intensity and peak shape even after prolonged pyridine intercalation (Fig. 5a-c). This finding and no observable change in thickness (AFM line scan in Figure 2c-d), imply that pyridine molecules do not diffuse between layers. As discussed before, this can be attributed to large Bohr radius of Te atoms resulting in stronger interlayer coupling, preventing pyridine molecules from diffusing. Interlayer coupling energy calculated from DFT results show that GaTe layers interact with each other $\sim 23\%$ stronger (-1.576 eV/nm² for GaSe, and -1.936 eV/nm² for GaTe) which is in accord with the discussions above.

Despite relatively unchanged PL spectrum of GaTe, its Raman spectrum undergoes a significant change as shown in Figure 5d. Raman spectrum of pristine GaTe is rather weak and displays broad peaks at 163 and 211 cm⁻¹. Interestingly, Raman intensity increases by two folds after intercalation, and concurrently series of new vibrational modes appear at 116, 129, 144, 178, 211, and 284 cm⁻¹. At first, these peaks might be interpreted as vibrational modes (signal) from byproduct materials (Te and Ga clusters)

created by presumably reactive interaction between pyridine and GaTe. However, our measurements on freshly exfoliated and mildly aged pristine GaTe samples reveal that P-GaTe Raman spectrum closely matches to that of freshly exfoliated GaTe samples, and observed peaks are related to 1st order Raman peaks of low-symmetry monoclinic phase of GaTe. GaTe surface is expected to physi-sorb O₂ molecules at the V_{Te} (Te vacancy sites), similar to MoTe₂.⁴⁶ Despite the exact origin is unknown, we speculate that improved environmental stability might be associated with passivating the defect sites, such as Te vacancies which can be easily oxidized in ambient condition, with pyridine molecules to avoid surface degradation. Previously, effects of Te vacancies on 2D materials (MoTe₂) have been discussed and our discussions are in line with earlier arguments⁴⁶. Here, we point that no observed changes in the flake thickness by AFM measurements suggest that the pyridine treatment does not coat GaTe surfaces, but instead might functionalize the defects sites. We also point out that since pyridine treatment largely changes the light emission properties of GaSe, it is rather difficult to distinguish surface effects from intercalation effects. This is also partly due to the fact that selenium compounds typically contain smaller density of defects as Te-based materials require higher temperature growth but possess lower material temperature (introducing Te-vacancies during cool-down process). In the view of this, we argue that extended stability of GaSe, with respect to GaTe, is related to intrinsic defects generated / present in typical material growth.

Overall results presented the first functionalization technique to control optical properties of both CVD grown and exfoliated gallium based post-transition metal chalcogenides (PTMCs), e.g. GaSe and GaTe, using pyridine (C₅H₅N) organic intercalant molecules. We find that pyridine molecules intercalate between GaSe layers, as evidenced by AFM and Raman spectroscopy measurements, thereby increasing PL intensity by introducing new bound exciton emission feature (mechanism). In contrast, due to strong interlayer coupling of GaTe, pyridine does not intercalate but instead treats GaTe surface in a way that it improves the environmental stability of GaTe. Findings offer a new way to manipulate the properties of quasi-2D PTMCs, which are potential candidates for energy harvesting, optoelectronics, and photonics applications owing to their reduced exciton binding energies in quasi-2D, direct gaps, and nearly-ideal band offset values for photoelectrochemical cell applications¹⁵.

Methods:

Material preparation and characterization: Crystalline GaSe and GaTe were grown using the Bridgman method. To study the optical changes in GaSe and GaTe layers after intercalation, both bulk crystals were separately used to mechanically exfoliate quasi-2D layers on 295 nm thick thermal SiO₂ on Si (SiO₂/Si) substrates. Following the exfoliation process, to achieve intercalation, GaSe and GaTe samples and a beaker of pyridine solution (0.5 ml) were then placed in a vacuum chamber, which was pumped and maintained at a pressure of 1 Torr, for 20 hours. As a result of low pressure, the vacuum chamber got filled with pyridine molecules for the span of intercalation process. A schematic for the intercalation setup and process is shown in Figure 1b. Structural evolution of the samples before and after intercalation was monitored by X-ray diffraction (XRD) technique using Cu K α irradiation on an 800 W

Philips 1830 powder diffractometer. Morphology and thickness variation before and after intercalation was characterized with Atomic Force Microscopy (AFM), scanned on a Bruker D3100 Scanning Probe Microscope in ambient environment. The scanning rate was 1Hz and resolution was set to 256×256. The data was processed using Gwyddion software. Optical changes were measured by Renishaw PL/Raman system. For both PL and Raman, a 488 nm source of laser was used as the excitation source. Time dependent PL slices were captured with an interval of 5 s between consecutive slices. Time dependent PL 3D map was collected after 60 PL spectra where each spectrum was averaged over 2-3 runs where each run lasted ~5 s, adding up to ~15 minutes collection.

DFT Calculations: To test the experimental results, we performed first-principle density functional band structure and total energy calculations. We have calculated the formation energy of pyridine-intercalated bilayer-GaSe and GaTe. The formation energy is defined as: $E_f = [E(\text{intercalated}) - E(\text{bilayer}) + E(\text{pyridine})]/S$, where $E(\text{intercalated})$, $E(\text{bilayer})$, and $E(\text{pyridine})$ are the total energies of the intercalated bilayer, the pristine bilayer, and the isolated pyridine molecule, respectively. S is the area of the bilayer in the supercell. In the calculations, a pyridine molecule is intercalated into a 2X2 supercell of bilayer GaSe, and a 2X1 supercell of GaTe.

References

1. W. Jie, X. Chen, D. Li, L. Xie, Y. Y. Hui, S. P. Lau, X. Cui and J. Hao, *Angew. Chemie International Edition*, 2015, **54**, 1185-1189.
2. L. Karvonen, A. Säynätjoki, S. Mehravar, R. D. Rodriguez, S. Hartmann, D. R. T. Zahn, S. Honkanen, R. A. Norwood, N. Peyghambarian, K. Kieu, H. Lipsanen and J. Riikonen, *Scientific Reports*, 2015, **5**, 10334.
3. X. Zhou, J. Cheng, Y. Zhou, T. Cao, H. Hong, Z. Liao, S. Wu, H. Peng, K. Liu and D. Yu, *Journal of the American Chemical Society*, 2015, **137**, 7994-7997.
4. Y. Ni, H. Wu, C. Huang, M. Mao, Z. Wang and X. Cheng, *Journal of Crystal Growth*, 2013, **381**, 10-14.
5. D. V. Rybkovskiy, N. R. Arutyunyan, A. S. Orekhov, I. A. Gromchenko, I. V. Vorobiev, A. V. Osadchy, E. Y. Salaev, T. K. Baykara, K. R. Allakhverdiev and E. D. Obraztsova, *Physical Review B*, 2011, **84**, 085314.
6. V. Zólyomi, N. D. Drummond and V. I. Fal'ko, *Physical Review B*, 2013, **87**, 195403.
7. O. D. Pozo-Zamudio, S. Schwarz, M. Sich, I. A. Akimov, M. Bayer, R. C. Schofield, E. A. Chekhovich, B. J. Robinson, N. D. Kay, O. V. Kolosov, A. I. Dmitriev, G. V. Lashkarev, D. N. Borisenko, N. N. Kolesnikov and A. I. Tartakovskii, *2D Materials*, 2015, **2**, 035010.
8. S. Lei, L. Ge, Z. Liu, S. Najmaei, G. Shi, G. You, J. Lou, R. Vajtai and P. M. Ajayan, *Nano Letters*, 2013, **13**, 2777-2781.
9. X. Li, M.-W. Lin, A. A. Puretzky, J. C. Idrobo, C. Ma, M. Chi, M. Yoon, C. M. Rouleau, I. I. Kravchenko, D. B. Geohegan and K. Xiao, *Sci. Rep.*, 2014, **4**, 5497.
10. Y. Ma, Y. Dai, M. Guo, L. Yu and B. Huang, *Physical Chemistry Chemical Physics*, 2013, **15**, 7098-7105.
11. L. Leontie, I. Evtodiev, V. Nedeff, M. Stamate and M. Caraman, *Applied Physics Letters*, 2009, **94**, 071903.

12. Z. Wang, M. Safdar, M. Mirza, K. Xu, Q. Wang, Y. Huang, F. Wang, X. Zhan and J. He, *Nanoscale*, 2015, **7**, 7252-7258.
13. D. J. Late, B. Liu, J. Luo, A. Yan, H. S. S. R. Matte, M. Grayson, C. N. R. Rao and V. P. Dravid, *Advanced Materials*, 2012, **24**, 3549-3554.
14. R. Le Toullec, N. Piccioli, M. Mejatty and M. Balkanski, *Il Nuovo Cimento B Series 11*, 1977, **38**, 159-167.
15. H. L. Zhuang and R. G. Hennig, *Chemistry of Materials*, 2013, **25**, 3232-3238.
16. H.-P. Komsa and A. V. Krasheninnikov, *Physical Review B*, 2012, **86**, 241201.
17. B. Zhu, X. Chen and X. Cui, *Sci. Rep.*, 2015, **5**, 9218.
18. K. He, N. Kumar, L. Zhao, Z. Wang, K. F. Mak, H. Zhao and J. Shan, *Phys. Rev. Lett.*, 2014, **113**, 026803.
19. A. Chernikov, T. C. Berkelbach, H. M. Hill, A. Rigosi, Y. Li, O. B. Aslan, D. R. Reichman, M. S. Hybertsen and T. F. Heinz, *Phys. Rev. Lett.*, 2014, **113**, 076802.
20. A. R. Klots, A. K. M. Newaz, B. Wang, D. Prasai, H. Krzyzanowska, J. Lin, D. Caudel, N. J. Ghimire, J. Yan, B. L. Ivanov, K. A. Velizhanin, A. Burger, D. G. Mandrus, N. H. Tolk, S. T. Pantelides and K. I. Bolotin, *Sci. Rep.*, 2014, **4**, 6608.
21. S. Tongay, W. Fan, J. Kang, J. Park, U. Koldemir, J. Suh, D. S. Narang, K. Liu, J. Ji, J. Li, R. Sinclair and J. Wu, *Nano Lett*, 2014, **14**, 3185-3190.
22. S. Tongay, J. Hwang, D. B. Tanner, H. K. Pal, D. Maslov and A. F. Hebard, *Physical Review B*, 2010, **81**, 115428.
23. J. Hwang, J. P. Carbotte, S. Tongay, A. F. Hebard and D. B. Tanner, *Physical Review B*, 2011, **84**, 041410.
24. S. Tongay, T. Schumann, X. Miao, B. R. Appleton and A. F. Hebard, *Carbon*, 2011, **49**, 2033-2038.
25. X. C. Miao, S. Tongay, M. K. Petterson, K. Berke, A. G. Rinzler, B. R. Appleton and A. F. Hebard, *Nano Letters*, 2012, **12**, 2745-2750.
26. J. Zheng, H. Zhang, S. Dong, Y. Liu, C. Tai Nai, H. Suk Shin, H. Young Jeong, B. Liu and K. Ping Loh, *Nat Commun*, 2014, **5**, 2995.
27. M. S. Dresselhaus and G. Dresselhaus, *Advances in Physics*, 1981, **30**, 139-326.
28. H. Fang, M. Tosun, G. Seol, T. C. Chang, K. Takei, J. Guo and A. Javey, *Nano Letters*, 2013, **13**, 1991-1995.
29. M. B. Dines, *Journal of Chemical Education*, 1974, **51**, 221.
30. M. S. Whittingham and R. R. Chianelli, *Journal of Chemical Education*, 1980, **57**, 569.
31. V. K. Lukyanuk and Z. D. Kovalyuk, *physica status solidi (a)*, 1987, **102**, K1-K5.
32. E. Jung, S. Lee, S. Roh, X. Meng, S. Tongay, J. Kang, T. Park and J. Hwang, *Journal of Physics D-Applied Physics*, 2014, **47**, 485304.
33. C. Lee, H. Yan, L. E. Brus, T. F. Heinz, J. Hone and S. Ryu, *ACS Nano*, 2010, **4**, 2695-2700.
34. H. Sahin, S. Tongay, S. Horzum, W. Fan, J. Zhou, J. Li, J. Wu and F. M. Peeters, *Physical Review B*, 2013, **87**, 165409.
35. J. C. Chacón-Torres, L. Wirtz and T. Pichler, *physica status solidi (b)*, 2014, **251**, 2337-2355.
36. J. J. Song, D. D. L. Chung, P. C. Eklund and M. S. Dresselhaus, *Solid State Commun.*, 1976, **20**, 1111-1115.

37. S. Tongay, J. Suh, C. Ataca, W. Fan, A. Luce, J. S. Kang, J. Liu, C. Ko, R. Raghunathanan, J. Zhou, F. Ogletree, J. B. Li, J. C. Grossman and J. Q. Wu, *Scientific Reports*, 2013, **3**, 2657
38. S. Tongay, J. Zhou, C. Ataca, J. Liu, J. S. Kang, T. S. Matthews, L. You, J. B. Li, J. C. Grossman and J. Q. Wu, *Nano Letters*, 2013, **13**, 2831-2836.
39. K. F. Mak, K. He, C. Lee, G. H. Lee, J. Hone, T. F. Heinz and J. Shan, *Nat Mater*, 2013, **12**, 207-211.
40. *Optical Properties of 2D Systems with Interacting Electrons*, Springer; Softcover reprint of the original 1st ed. 2003 edition (October 31, 2003).
41. E. Bianco, S. Butler, S. Jiang, O. D. Restrepo, W. Windl and J. E. Goldberger, *ACS Nano*, 2013, **7**, 4414-4421.
42. O. I. Joshua, A. S. Gary, S. J. v. d. Z. Herre and C.-G. Andres, *2D Materials*, 2015, **2**, 011002.
43. A. Acun, B. Poelsema, H. J. W. Zandvliet and R. van Gastel, *Applied Physics Letters*, 2013, **103**, 263119.
44. J. Kang, S. Tongay, J. B. Li and J. Q. Wu, *J. Appl. Phys.*, 2013, **113**, 143703.
45. S. Horzum, D. Cakir, J. Suh, S. Tongay, Y. S. Huang, C. H. Ho, J. Wu, H. Sahin and F. M. Peeters, *Physical Review B*, 2014, **89**, 115407.
46. B. Chen, H. Sahin, A. Suslu, L. Ding, M. I. Bertoni, F. M. Peeters and S. Tongay, *ACS Nano*, 2015, **9**, 5326-5332.